BJRS

BRAZILIAN JOURNAL
OF
RADIATION SCIENCES
10-02A (2022) 01-18

Plastic bottle caps as radiation detectors for high gamma radiation doses

Oliveira[a,b,*] L.N., Nascimento[a] E.O., Antonio[b] P.L., and Caldas[b] L.V.E

[a] *Instituto Federal de Educação, Ciência e Tecnologia de Goiás –IFG, Goiânia - GO, Brazil*

[b] *Instituto de Pesquisas Energéticas e Nucleares – IPEN/CNEN, São Paulo - SP, Brazil*

lucas@ifg.edu.br

ABSTRACT

Dosimetric evaluation is indicated for material characterization seeking to identify possible applications; still, proper preprocessing techniques are critical features of this process. This work aimed to determine the linearity response of plastic samples irradiated with gamma rays using the Fourier Transform Infrared (FTIR) measurements. The plastic samples were analyzed using Derivatives and Principal Component Analysis (PCA) methods. They applied linear and Principal Component Regression (PCR) methods to obtain linearity. The methods obtained good results for linearity and also showed the evolution of each technique. In conclusion, the results indicate that the applied methods can be useful in radiation physics and for plastic samples as interesting potential radiation detectors.

Keywords: **Plastic samples, Radiation dosimetry, PCR analyses, FTIR technique**

ISSN: 2319-0612
DOI: https://10.15392/bjrs.v10i2A.1761
Submitted:2021-11-05
Accepted: 2022-03-14

1. INTRODUCTION

Plastic dosimeters represent an important role in radiation applications [1–5]. They have been used in a variety of applications, such as portal monitors [6], solar radiation[7], radiation attenuation [8], cosmic radiation [9], UV radiation [10], thermal radiation [11] and gamma radiation [12–14].

The Fourier Transform Infrared (FTIR) reading technique has been used to measure the sample surface absorbance in evaluating plastic detectors. The FTIR has been applied recently in several areas [15–20].

One of the most desired dosimetric characteristics, whether for plastic or any other detector, is the prevalence of linearity of response regarding the absorbed dose profiles. In several circumstances, linearity response can be found directly from the raw data without preprocessing [21–25]. Although the direct method cannot identify linear behavior, other methods can be used to transform the raw data into a different metric space.

Consequently, there are several spectrum preprocessing methods such as higher-order derivatives [26,27], Fast Fourier Transform (FFT) [28], Principal Component Analysis (PCA) method [29,30] and the use of autoencoder in artificial neural network [31]. Onwards, linearity can be determined through several methods, the most common being the ordinary Linear Regression (LR) method. Nevertheless, other robust approaches are being applied, as the Principal Component Regression (PCR) [32–36]. PCR can be understood with exactly two steps, the first is the application of the PCA and soon after the regression which will provide the main components for a new explanatory variable in the model [37]. More information on the application of PCR in dosimetry can be found in the literature [38].

The objective of this work was to evaluate Polyethylene Terephthalate/F217 (PET) samples exposed to gamma radiation as a linear radiation detector when exposed to gamma radiation. The FTIR and its first and second derivatives were used as preprocessing techniques. After assessing linearity, the LR was employed in the FTIR derivatives, and PCR was applied directly in the FTIR spectra.

2. MATERIALS AND METHODS

Bottle plastic screw caps (white color) were used as sample detectors. The samples were composed of a hollow cylindrical shape with a 14 mm radius, 0.05 mm thickness, and 28 mm height, weigh of 3.1 g and polyethylene (F217). These samples were irradiated in triplicates, with absorbed doses of 0.01 kGy, 0.05 kGy, 0.10 kGy, 0.25 kGy, 0.50 kGy, 1.0 kGy, 5.0 kGy and 10.0 kGy using a ^{60}Co Gamma Cell-220 system (dose rate of 1.089 kGy/h at the Radiation Technology Center of IPEN). Afterwards, the absorbance spectrum of each sample was acquired on a Fourier Transform Infrared (FTIR) Spectrometer (Frontier/Perkin Elmer) from 400 cm^{-1} to 4000 cm^{-1}, with a 1 cm^{-1} spectral resolution. The FTIR technique is non-destructive, fast, and presents an excellent spatial resolution in the plastic sample measurements.

The preprocessing was performed in the raw data composed by the broadband source interferogram with a +/- 0.04 cm-1 (2σ) precision for each absorbed dose profile. Subsequently, applying the Fast Fourier Transform (FFT), FTIR was generated and from that, the derivates in the frequency (wavenumber) space were calculated seeking to assess high-order effects. After, the complex FFT coefficients were explicitly obtained for peak regions, which provide localized information regarding the approximate spectrum shape from the FTIR evaluations to find linearity estimatives.

The resulting FTIR spectrum for each peak went to numerical differentiation at the 1st, 2nd and 3 rd orders (D1, D2 and D3, respectively). The derivates obtained were useful in getting the shapes of the spectrum and their linearity. Within the identified peak region, a linear regression was performed at each fixed wavenumber. The absorbed doses were used as the regressor variables and the corresponded absorbance value as the independent variable. The squared Pearson correlation coefficient, called linearity (R^2) was determined.

The PCA method can reduce the whole FTIR dimension but it preserves the original information. PCA analysis was used to obtain linearity through the application of the PCR method. The PCR method consists of choosing the number of principal components (k = 1 up to k = 8) associated with the variance of the absorbance and the absorbed doses matrix. The Mean Squared Error (MSE) was used to calculate the PCR method prediction accuracy, given the choice of the best k value, then the linear regression is performed. The multivariate analysis was applied in Matlab 2020a.

3. RESULTS AND DISCUSSION

The absorbance *versus* wavenumber results for plastic samples irradiated with absorbed doses from 0.01 kGy to 10.0 kGy (^{60}Co source) are presented in: Fig. 1a) total, Fig. 1b) I, Fig. 1c) II and Fig. 1d) III regions, for FTIR spectra. The three regions were analyzed to guarantee the absorbance value change visualization with the dose absorbance. The samples did not change their color because of irradiation. For the Raw method data, it was impossible to find good linearity values, thus requiring other methods and preprocessing for this objective. From these results, the vibrational mode for C-H asymmetric and symmetrical stretching at 2915 and 2846 cm^{-1} respectively can be inferred too.

a)

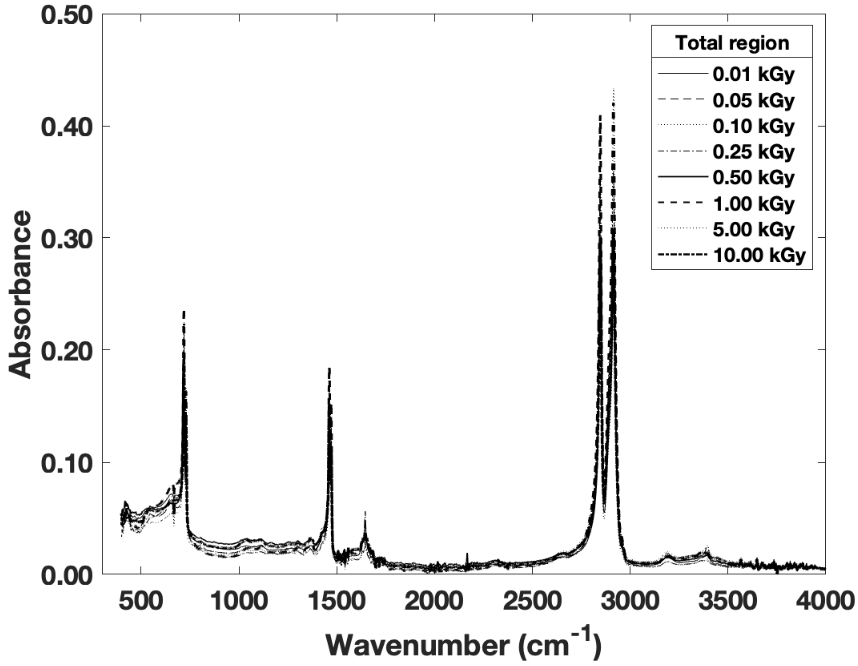

b)

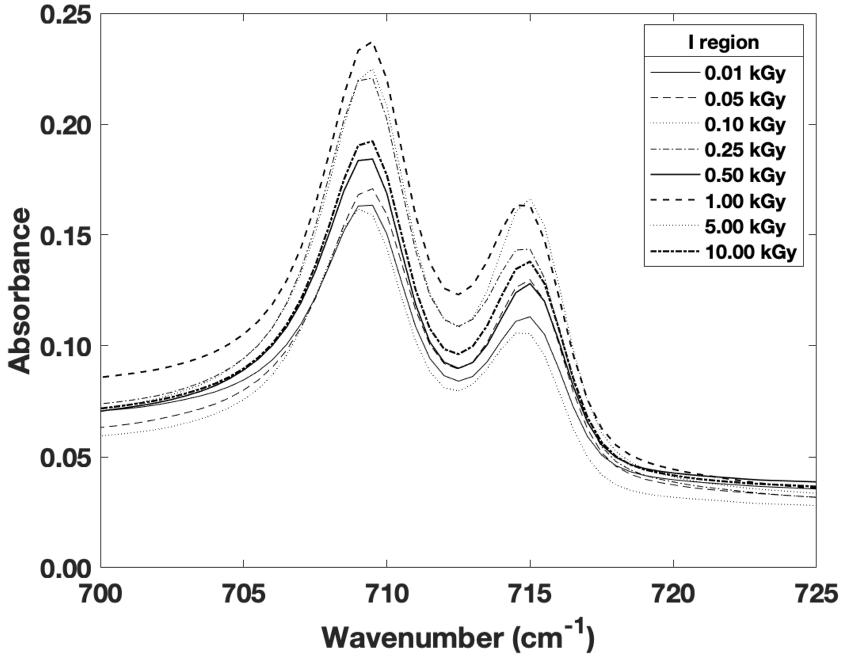
I region
0.01 kGy
0.05 kGy
0.10 kGy
0.25 kGy
0.50 kGy
1.00 kGy
5.00 kGy
10.00 kGy
Absorbance
Wavenumber (cm-1)
0.00
0.05
0.10
0.15
0.20
0.25
700
705
710
715
720
725

c)

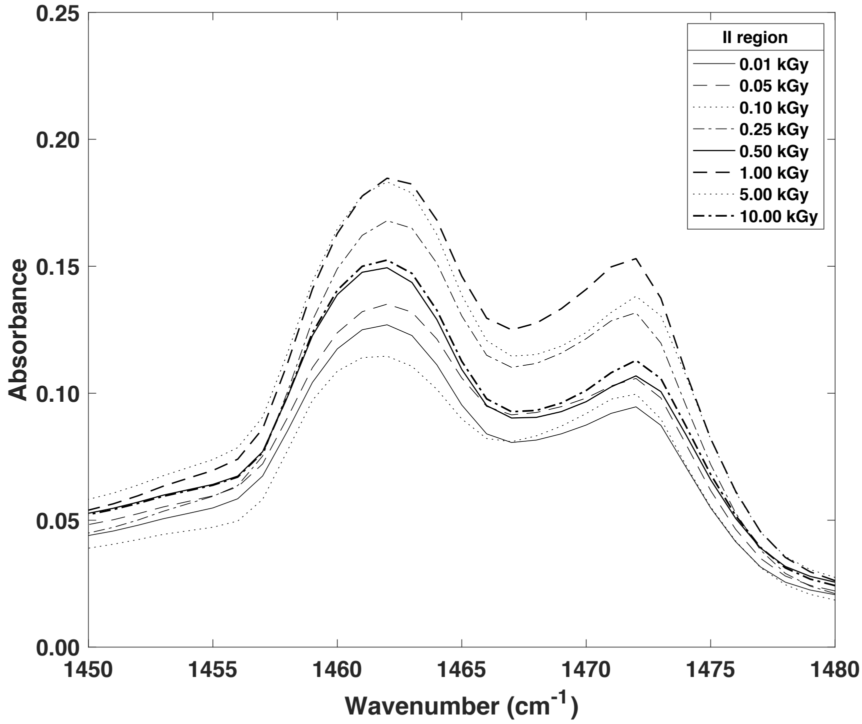
II region
0.01 kGy
0.05 kGy
0.10 kGy
0.25 kGy
0.50 kGy
1.00 kGy
5.00 kGy
10.00 kGy
Absorbance
Wavenumber (cm-1)
0.00
0.05
0.10
0.15
0.20
0.25
1450
1455
1460
1465
1470
1475
1480

d)

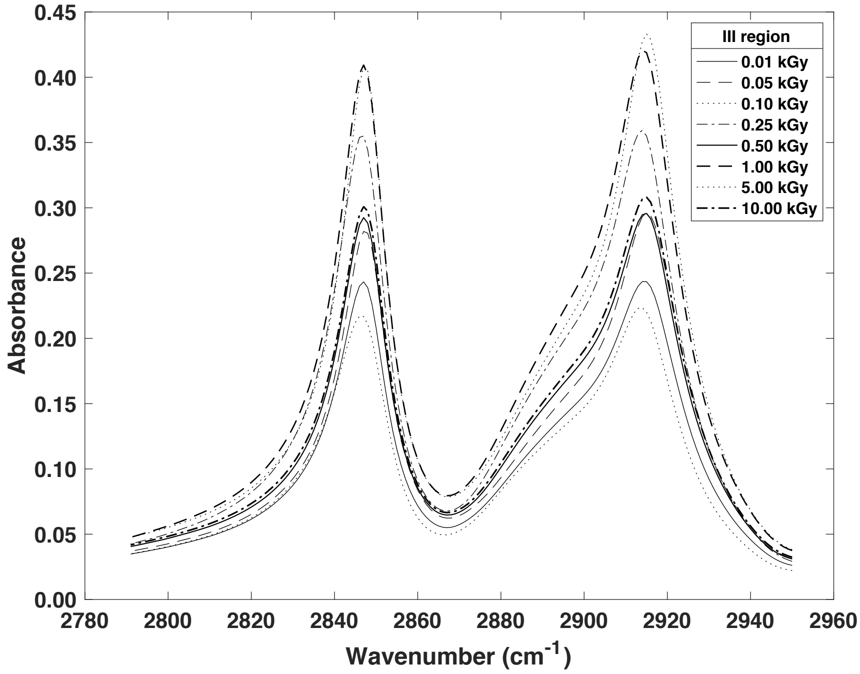

Figure 1: *Absorbance versus wavenumber, for plastic samples irradiated with absorbed doses from 0.01 kGy to 10.0 kGy (^{60}Co source): a) total, b) I, c) II and d) III regions for FTIR spectra. The average of 3 samples was evaluated for each curve, and the uncertainty obtained was lower than 1%.*

Results about imaginary *versus* real parts of the Fourier transform (coefficients) of spectra are shown on the left side in Fig 2, and to the right side the FFT amplitude *versus* wavenumber is shown for all absorbed doses for plastic samples. Based on the coefficients, it is possible to build the plastic sample Fourier spectrum function. Another detail is the right side of each figure; it describes the coefficient real part, and all the results indicate that Gaussian distributions could explain the spectra. Although the previous results are significant (left side for Fig.2), the FFT amplitudes obtained showed peaks with high amplitude, and it is possible even to observe the variation of the absorbed doses. However, for the FFT amplitude, few wavenumbers are needed to obtain it. Since the analyzed spectrum (Fig. 1) has ups and downs in a minimal range of wavenumbers, the amplitudes tended to zero. Because of this scenario, the application for the approximation of spectra was not suitable for this work in linearity applications to plastic samples.

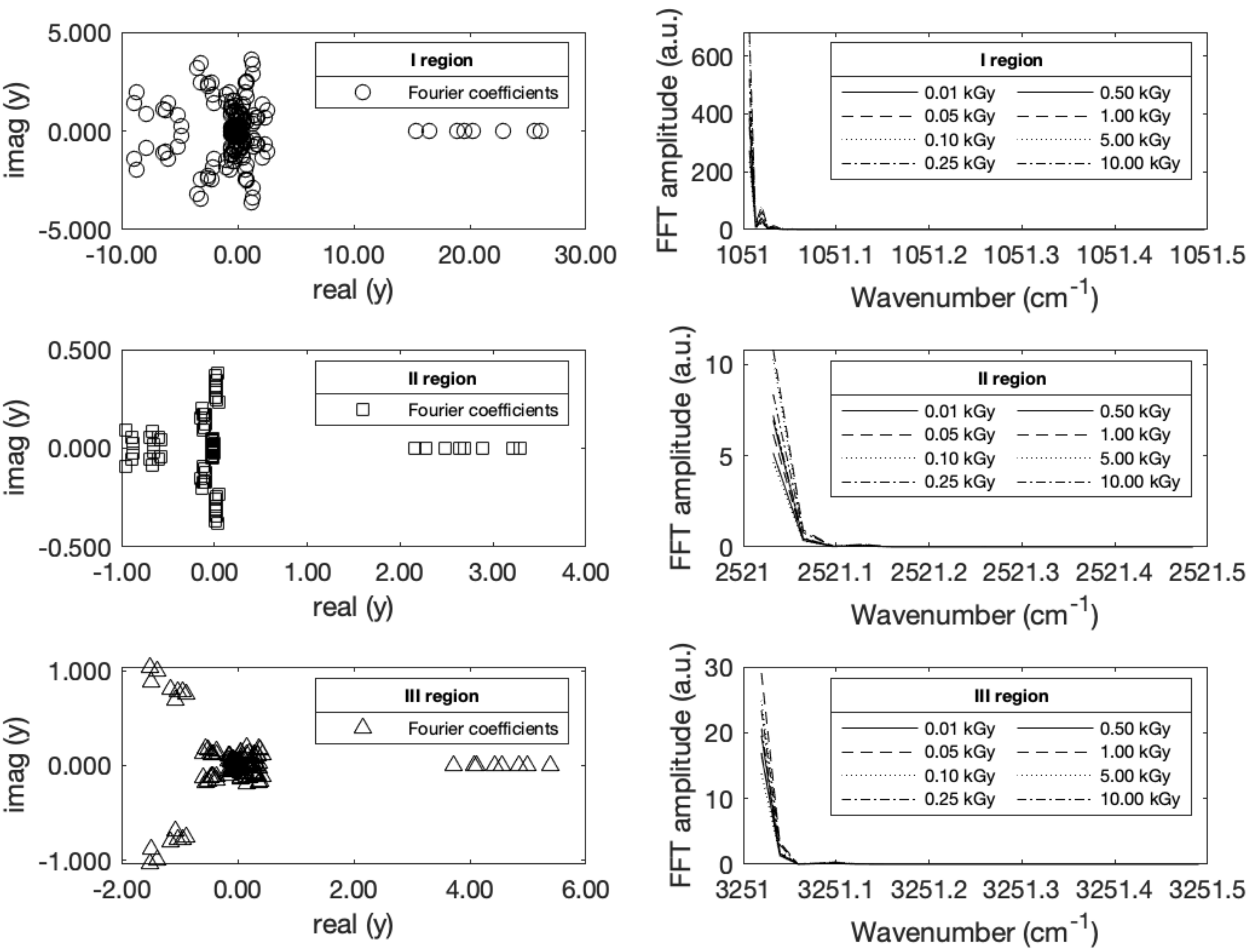

Figure 2: *On the left side: Imaginary versus real parts of the Fourier transform (coefficients) of spectra. On the right side: FFT amplitude versus wavenumber for all absorbed doses.*

The absorbance derivative results *versus* absorbance to the left side and absorbance versus wavenumber to the right side are presented at: Fig. 3a) I, Fig. 3b) II and Fig. 3c) III regions for plastic samples, and for 0.01 kGy absorbed dose. For all the analyzed regions it was possible to infer that for D1, the negative values of the derivative provided negative absorbance values. This is associated with a discrete function, which is already discarded in radiation dosimetry, because for a detector the function of its readings must be proportional to the absorbed doses, while the D2 and D3 both provided positive values for absorbance, but then positive functions. Based on this positive function growth, it was possible to obtain values for linearity > 0.7515 and > 0.5857, respectively, for D2 and D3.

a)

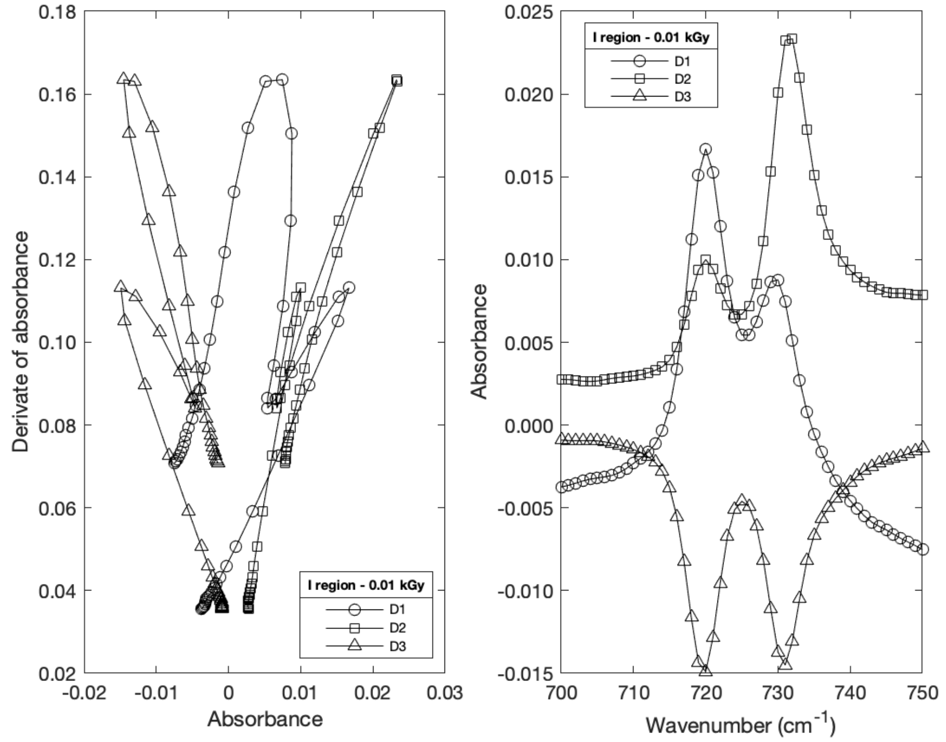
Derivate of absorbance
Absorbance
I region - 0.01 kGy
D1
D2
D3
Absorbance
Wavenumber (cm^{-1})
I region - 0.01 kGy
D1
D2
D3

b)

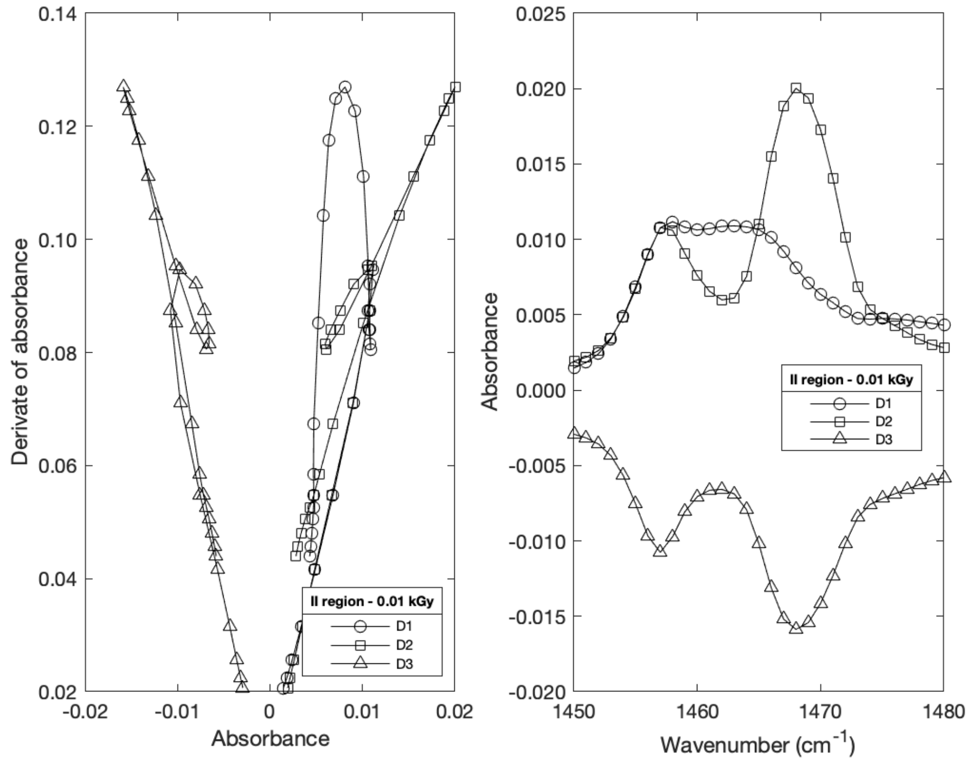
Derivate of absorbance
Absorbance
II region - 0.01 kGy
D1
D2
D3
Absorbance
Wavenumber (cm^{-1})
II region - 0.01 kGy
D1
D2
D3

c)

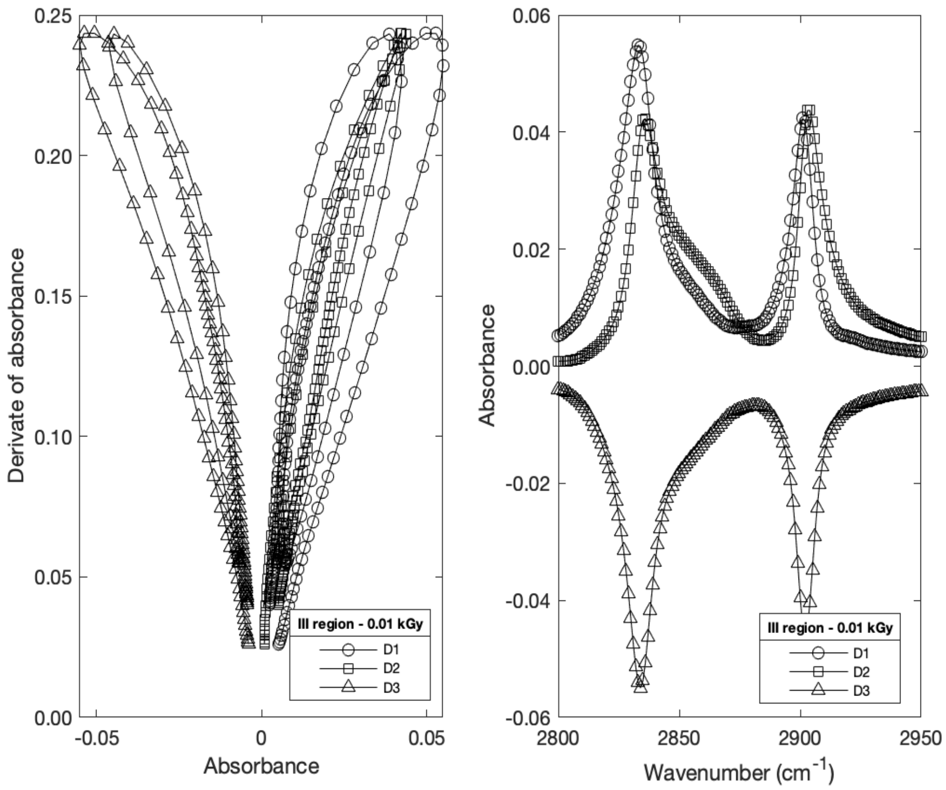

Figure 3: *Derivate of the absorbance versus absorbance to the left side, and absorbance versus wavenumber to the right side: a) I, b) II and c) III regions for plastic samples, and all absorbed doses. The uncertainty obtained was lower than 1%.*

Figures 4a, 4b and 4c present the absorbance *versus* linearity results for plastic samples and with D2, D3, D1, FFT and Raw preprocessing in ascending order: I, II and III regions for 0.01 kGy, 0.25 kGy and 10.0 kGy, respectively. The three absorbed doses (0.01 kGy, 0.25 kGy, and 10.0 kGy), with the three regions under study, were chosen to verify that the methods can be applied to all values of absorbed doses and regions. For all regions, the highest values of linearity were: D2 > D3 > D1 > FFT > Raw. So far, linearity values were obtained with preprocessing and linear methods that are quick to perform.

a)

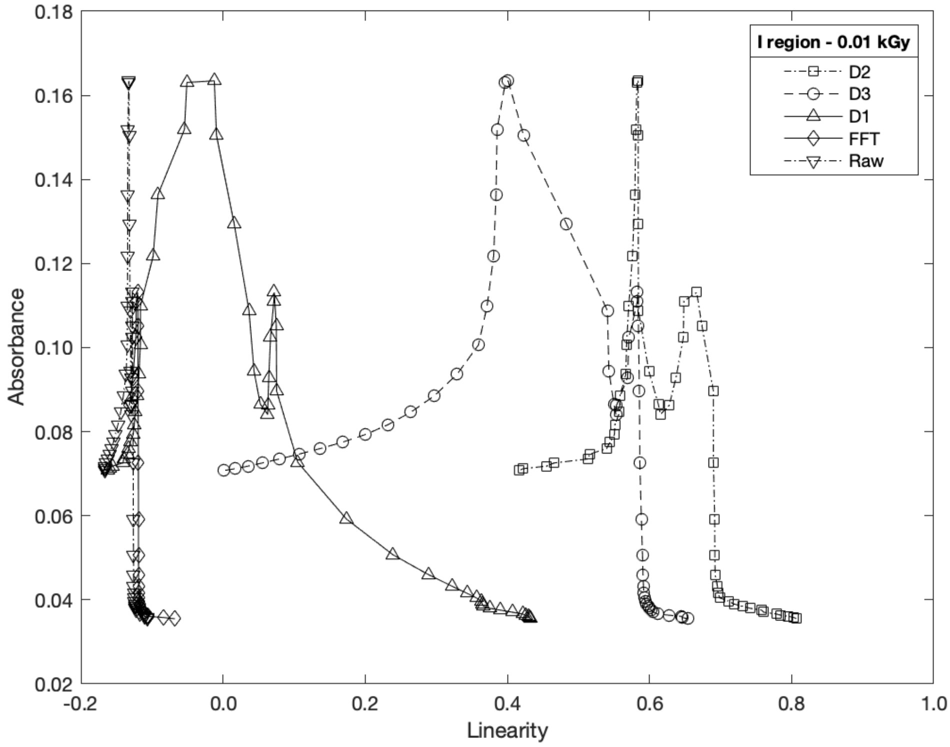
I region - 0.01 kGy
D2
D3
D1
FFT
Raw
Absorbance
Linearity
0.18
0.16
0.14
0.12
0.10
0.08
0.06
0.04
0.02
-0.2
0.0
0.2
0.4
0.6
0.8
1.0

b)

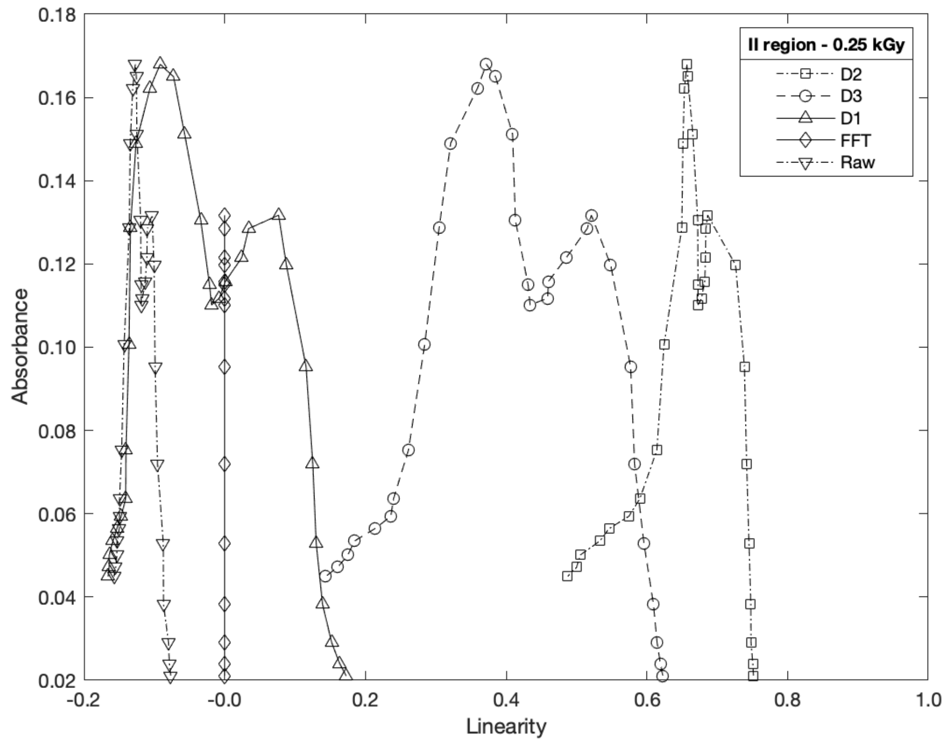
II region - 0.25 kGy
D2
D3
D1
FFT
Raw
Absorbance
Linearity
0.18
0.16
0.14
0.12
0.10
0.08
0.06
0.04
0.02
-0.2
-0.0
0.2
0.4
0.6
0.8
1.0

c)

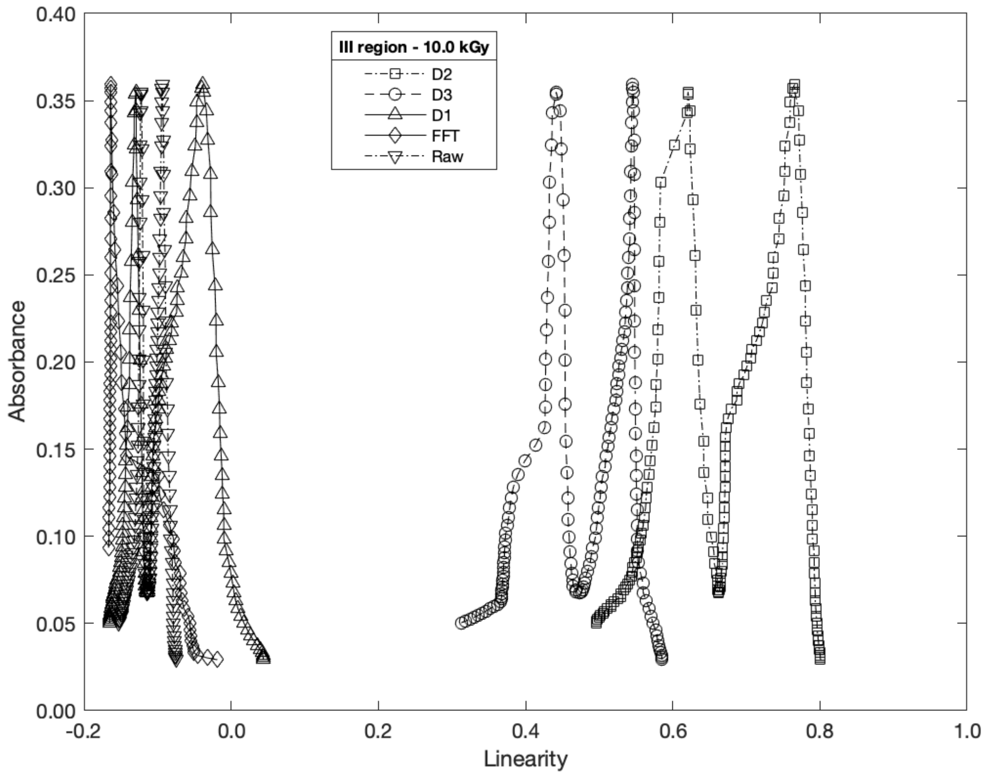

Figure 4: *Absorbance versus linearity for plastic samples, and with D2, D3, D1, FFT and Raw preprocessing in ascending order: a) I, b) II and c) III regions for 0.01 kGy, 0.25 kGy and 10.0 kGy, respectively. The uncertainty obtained was lower than 1%.*

Figure 5 presents the application of the PCR method: Predicted absorbed dose *versus* absorbed dose, for: I, II and III regions. The results of the PCR method are the maximum values for linearity, 1.000 for all regions. This result demonstrates that the PCR method is more robust than the linear method, and the preprocessing via PCA kept the information pertinent to the evaluated plastic detector.

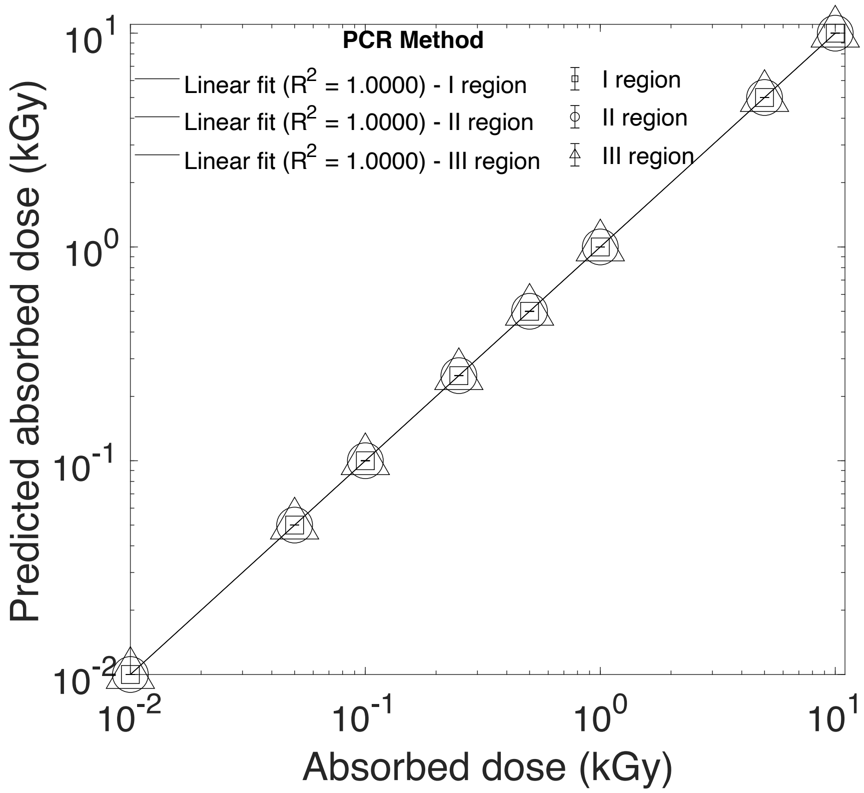

Figure 5: *Application of the PCR method: Predicted absorbed dose versus absorbed dose; for: I, II and III regions. The uncertainty obtained was lower than 1%.*

The Mean-Squared Error (MSE) results *versus* the number of principal components for the PCR method are shown in Fig. 6. For all regions, the MSE values decrease with the increase in *k* values. In this work, the chosen value of *k* was 8 to obtain a zero value for the MSE.

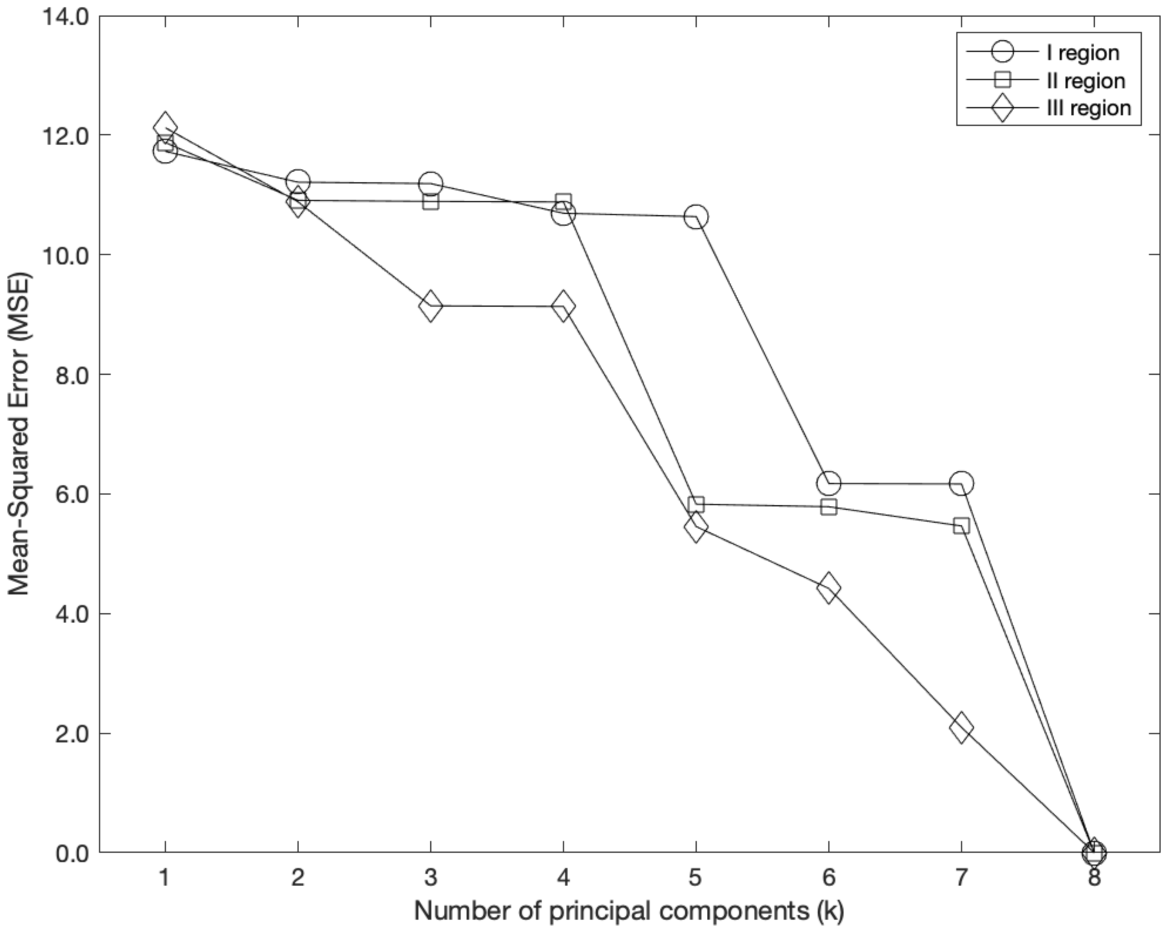

Figure 6: *Mean-Squared Error (MSE) versus number of principal components (k) for PCR method and all regions. The uncertainty obtained was lower than 1%.*

Table 1 shows the linearity comparison of six preprocessing methods in ascending order: Raw, FFT, D1, D3, D2 and PCA, associated with linear and PCR methods and for all regions. The highest values of linearity were for all regions: PCA > D2 > D3 > D1 > FFT > Raw pre-processing. The addition of PCA and PCR methods indicates that they are more robust compared to the other methods. However, they need more time to be carried out in comparison to the other methods.

Table 1: Linearity comparison of six preprocessing methods in ascending order: Raw, FFT, D1, D3, D2 and PCA, associated with linear and PCR methods and for all regions.

		Linearity (R^2)		
Method	**Pre-processing**	**I region**	**II region**	**III region**
Linear	Raw	-0.0744	-0.0766	-0.1058
Linear	FFT	-0.0187	0.0000	0.0000
Linear	D1	0.0439	0.1727	0.4330
Linear	D3	0.5857	0.6228	0.6536
Linear	D2	0.8008	0.7515	0.8065
PCR	PCA	1.0000	1.0000	1.0000

4. CONCLUSION

In this work, from the information obtained about the investigation of plastic detectors with linearity values, data preprocessing and FTIR measurements, it can be concluded that: i) the FTIR technique was adequate in the application of the evaluation of solid-state detectors such as plastic samples; ii) preprocessing methods can be used to obtain linearity in irradiated plastic samples; iii) for linearity, the PCR method showed better results than the linear model in all regions of the spectra.

In conclusion, dosimetric characteristics are useful for the radiation dosimetry area, such as linearity, and plastic samples are a potential radiation detector.

ACKNOWLEDGMENTS

The authors thank the Brazilian funding agencies CNPq (Projects 104486/2019-8, 164981/2020-9, 151945/2019-5 and 301335/2016-8) and FAPESP (Projects 2018/05982-0 and 2014/12732-9) for partial financial support.

REFERENCES

[1] LEE, C.K.; WONG, H.K.; LEUNG, Y.L. Non-linearity of pre-dose response and its effects on TL dating. **Radiat Meas,** v. 44, p. 215-222, 2009.

[2] MADDEN, L.; ARCHER, J.; LI, E.; JELEN, U.; DONG, B.; HOLLOWAY, L.; *et al*. MRI-LINAC beam profile measurements using a plastic scintillation dosimeter. **Phys Med,** v. 73, p. 111-116, 2020.

[3] POSAR, J.A.; DAVIS, J.; BRACE, O.; SELLIN, P.; GRIFFITH, M.J.; DHEZ, O.; *et al*. Characterization of a plastic dosimeter based on organic semiconductor photodiodes and scintillator. **Phys Imaging Radiat Oncol,** v. 14, p. 48-52, 2020.

[4] SOHRABPOUR, M.; KAZEMI, A.A.; MOUSAVI, H.; SOLATI, K. Temperature response of a number of plastic dosimeters for radiation processing. **Radiat Phys Chem,** v. 42, p. 783-787, 1993.

[5] WUU, C.S.; XU, Y. 3-D dosimetry with optical CT scanning of polymer gels and radiochromic plastic dosimeter. **Radiat Meas,** v. 66, p. 1903-1907, 2011.

[6] IHANTOLA, S.; HOLM, P.; JUTILA, H.; PERÄJÄRVI, K. Method for the diagnosis of aged plastic radiation portal monitors. **Appl Radiat Isot,** v. 160, 1-6, 2020.

[7] SERRANO, M.A.; MORENO, J.C. Spectral transmission of solar radiation by plastic and glass materials. **J Photochem Photobiol B Biol,** v. 208, p. 1-11, 2020.

[8] KOVACEVIC, M.S.; SAVOVIC, S.; DJORDJEVICH, A.; BAJIC, J.; STUPAR, D.; *et al*. Measurements of growth and decay of radiation induced attenuation during the irradiation and recovery of plastic optical fibres. **Opt Laser Technol,** v. 47, p. 148-151, 2013.

[9] AMBROZOVA, I.; BRABCOVA, K.P.; KUBANCAK, J.; ŠLEGL, J.; TOLOCHEK, R.V.; *et al*. Cosmic radiation monitoring at low-Earth orbit by means of thermoluminescence and plastic nuclear track detectors. **Radiat Meas,** v. 106, p. 262-266, 2017.

[10] SUHRHOFF, T.J.; SCHOLZ-BÖTTCHER, B.M. Qualitative impact of salinity, UV radiation and turbulence on leaching of organic plastic additives from four common plastics - A lab experiment. **Marine Pollut Bull,** v. 102, p. 84-94, 2016.

[11] SADOOGHI, P. Transient thermal radiation heat transfer in a reinforced plastic coating with anisotropic optical properties. **Int J Heat Mass Transf,** v. 123, p. 432-436, 2018.

[12] KARINA, K.M.; NAPOLITANO, C.M.; BORRELY, S.I. Gamma radiation effects in packaging for sterilization of health products and their constituents paper and plastic film. **Radiat Phys Chem,** v. 142, p. 23-28, 2018.

[13] KIM, D.; LEE, S.; PARK, J.; SON, J.; KIM, T.H.; KIM, Y.H.; *et al*. Performance of 3D printed plastic scintillators for gamma-ray detection. **Nucl Eng Technol,** v. 243, p. 34-39, 2020.

[14] TAJUDIN, S.M.; NAMITO, Y.; SANAMI, T.; HIRAYAMA, H. Response of plastic scintillator to gamma sources. **Appl Radiat Isot,** v. 159, 1-8, 2020.

[15] AYDIA, M.I.; HIEKAL, A.S.; EL-AZONY, K.M.; MOHAMED, T.Y.; SHAHIN, I.M. Preparation and characterization of poly nano-cerium chloride for ^{99}Mo production based on neutron activation reactions. **Appl Radiat Isot,** v. 163, 1-11, 2020.

[16] KARELIN, A.I.; KAYUMOV, R.R.; DOBROVOLSKY, Y.A. FTIR spectroscopic study of the interaction between NH^{4+} and DMSO in Nafion. **Spectrochim Acta A Mol Biomol Spectrosc,** v. 215, 381-388, 2019.

[17] KAUR, S.; SINGH, S.; SINGH, L. Opto-electric and physio-chemical changes in oxygen ion irradiated natural Vermiculite mineral. **Appl Radiat Isot,** v. 148, 7-12, 2019.

[18] OLIVEIRA, L.N.; SCHIMIDT, F.; ANTONIO, P.L.; ANDREETA, M.R.B.; CALDAS, L.V.E. Lithium diborate glass for high-dose dosimetry using the UV-Vis and FTIR spectrophotometry techniques. **Radiat Meas,** v. 106, p. 225-228, 2017.

[19] RAMKUMAR, P.L.; PANCHAL, Y.; PANCHAL, D.; GUPTA, N. Characterization of LLDPE/coir blend using FTIR technique. **Mater Today: Proc,** v. 1, p. 1-5, 2020.

[20] RIHAWY, M.S.; ALZIER, A.; ALLAF, A.W. Investigation of chloramphenicol release from PVA/CMC/HEA hydrogel using ion beam analysis, UV and FTIR techniques. **Appl Radiat Isot,** v. 153, 1-8, 2019.

[21] BALAGHI, S.; GHAL-EH, N.; MOHAMMADI, A.; VEGA-CARRILLO, H.R. A neutron scattering soil moisture measurement system with a linear response. **Appl Radiat Isot,** v. 142, 167-172, 2018.

[22] DATZ, H.; HOROWITZ, Y.S.; OSTER, L.; MARGALIOT, M. Critical dose threshold for TL dose response non-linearity: Dependence on the method of analysis: It's not only the data. **Radiat Meas,** v. 46, p. 1444-1447, 2011.

[23] POMME, S.; PAEPEN, J.; VAN AMMEL, R. Linearity check of an ionisation chamber through 99 mTc half-life measurements. **Appl Radiat Isot,** v. 140, p. 171-178, 2018.

[24] SANI, S.F.A.; OTHMAN, M.H.U.; ALQAHTANI, A.; NAZERI, A.A.Z.A.; ALMUGREN, K.S.; UNG, N.M.; *et al*. Passive dosimetry of electron irradiated borosilicate glass slides. **Radiat Phys Chem,** v. 178, p. 1-8, 2020.

[25] ZAKARIA, Z.; AZIZ, M.Z.A.; ISHAK, N.H.; SUPPIAH, S.; BRADLEY, D.A.; NOOR, N.M. Advanced thermoluminescence dosimetric characterization of fabricated Ge-Doped optical fibres (FGDOFs) for electron beams dosimetry. **Radiat Phys Chem,** v. 166, p. 1-7, 2020.

[26] CHEN, S.J.; PENG, C.J.; CHEN, Y.C.; HWANG, Y.R.; LAI, Y.S.; FAN, S.Z.; *et al*. Comparison of FFT and marginal spectra of EEG using empirical mode decomposition to monitor anesthesia. **Comput Methods Programs Biomed,** v. 137, 77-85, 2016.

[27] SANCHEZ ROJAS, F.; BOSCH OJEDA, C. Recent development in derivative ultraviolet/visible absorption spectrophotometry: 2004-2008. A review. **Anal Chim Acta,** v. 635, p. 22-44, 2009.

[28] PENG, B.; GAO, C.; ZHOU, Y.; GUO, Y. Temperature-compensated ppb-level sulfur dioxide detection system based on fourier transform ultraviolet differential optical absorption spectrum method. **Sens Actuators B Chem,** v. 312, p. 1-8, 2020.

[29] FOLCH-FORTUNY, A.; ARTEAGA, F.; FERRER, A. PCA model building with missing data: New proposals and a comparative study. **Chemometr Intell Lab Syst,** v. 146, p. 77-88, 2015.

[30] LEVADA, A.L.M. Parametric PCA for unsupervised metric learning. **Pattern Recognit Lett,** v. 135, 425-430, 2020.

[31] GHOLIPOUR PEYVANDI, R.; ISLAMI RAD, S.Z. Precise prediction of radiation interaction position in plastic rod scintillators using a fast and simple technique: Artificial neural network. **Nucl Eng Technol,** v. 50, p. 1154-1159, 2018.

[32] AMIT, J.R.; KUMARI, S.; KELLY, S.; CANNAVAN, A.; SINGH, D.K. Rapid detection of pure coconut oil adulteration with fried coconut oil using ATR-FTIR spectroscopy coupled with multivariate regression modelling. **LWT,** v. 125, p. 1-10, 2020.

[33] BATISTA BRAGA, J.W.; ALLEGRINI, F.; OLIVIERI, A.C. Maximum likelihood unfolded principal component regression with residual bilinearization (MLU-PCR/RBL) for second-order multivariate calibration. **Chemometr Intell Lab Syst,** v. 170, p. 51-57, 2017.

[34] LI, X.; ZHANG, C.; BEHRENS, H.; HOLTZ F. Calculating biotite formula from electron microprobe analysis data using a machine learning method based on principal components regression. **Lithos**, v. 356, p. 1-12, 2020.

[35] SOLANKI, R.B.; KULKARNI, H.D.; SINGH, S.; VERMA, A.K.; VARDE, P. Optimization of regression model using principal component regression method in passive system reliability assessment. **Prog Nucl Energy,** v. 103, p. 126-134, 2018.

[36] URBANSKI, P. Principal component and partial least squares regressions in the calibration of nucleonic gauges. **Appl Radiat Isot,** v. 45, p. 659-667, 1994.

[37] KAWANO, S.; FUJISAWA, H.; TAKADA, T.; SHIROISHI, T. Sparse principal component regression for generalized models. **Comput Stat Data Anal**, v. 124, p. 180-196, 2018.

[38] OLIVEIRA, L.N.; NASCIMENTO, E.O.; MORAIS JÚNIOR, P.A.; ANTONIO, P.L; CALDAS, L.V.E. Evaluation of high-linearity bone radiation detectors exposed to gamma-rays via FTIR measurements. **Appl Radiat Isot**, v. 170, p. 1-6, 2021.